Creating diamond color centers for quantum optical applications

Creation of high density ensembles of nitrogen vacancy centers in diamond

F. C. Waldermann,* J. Nunn, K. Surmacz, Z. Wang, D. Jaksch, R. A. Taylor, and I. A. Walmsley

Clarendon Laboratory, University of Oxford, Parks Road, Oxford, OX1 3PU, UK

P. Olivero, M. Draganski, B. Fairchild, P. Reichart, A. Greentree, D. Jamieson, and S. Prawer

Centre for Quantum Computer Technology and School of Physics, Microanalytical Research Centre, The University of Melbourne, Parkville, Victoria 3010, Australia

Abstract

Nitrogen vacancy (NV) centers in diamond appear as quantum absorbers that are suitable for quantum information processing (QIP) due to their Λ-shaped energy structure. Procedures for their creation in high pressure high temperature (HPHT) diamond exist and could be used for QIP using ensembles of NV centers. However, the creation of ultra-high densities of NV centers by ion irradiation suffers from concurrent damage to the diamond crystal, which could impose limits on the optical accessibility and the temporal stability of the absorbers created. In our work, we employ systematic high energy ion implantation to nitrogen-rich HPHT diamond to create ensembles with various densities of NV centers. Using microphotoluminescence, these NV ensembles are analyzed with respect to their luminescence intensities, charge states and linewidths. We find conditions for which the NV centers are in a stable charge state and the material absorption is negligible, while ultra-high densities of NV centers are achieved. These results are reviewed in the context of quantum information processing. In particular, we analyze the suitability of the negatively charged NV center for an off-resonant, unitary photon memory scheme.

PACS numbers: 61.72.-y, 61.72.Ww, 71.55.-i, 78.55.-m

Keywords: diamond impurities, ion implantation, optical properties characterization, quantum information processing

I. INTRODUCTION

The creation of single photoluminescence centers in diamond has promising applications in the development of hybrid optical solid state quantum devices. Diamond exhibits a large inventory of optically active centers, related to the vibrational and electronic states of impurities and defects in the crystal lattice[1]. In particular, in a series of remarkable experiments the nitrogen-vacancy (NV) center demonstrated a great potential for single photon generation[2], quantum cryptography[3] and spin-based quantum computation[4]. Based on such promising proof-of-principle results, several different schemes have been proposed for quantum information processing in NV diamond systems, namely, Stark tuning, resonant dipole-dipole coupling, weak non-linearities, repeat-until-success and brokered graph states[5].

The realization of scalable devices for the above-mentioned applications requires adequate control on the formation process of active NV centers in diamond crystals. Two alternative routes are available for the creation of NV centers: radiation damage from various sources (ions, electrons, neutrons, etc.) to create vacancies in nitrogen-rich (i.e. type Ib) diamond, and direct implantation of nitrogen in the purest (i.e. type IIa) crystals. Arguably, it is the latter strategy that will ultimately represent the most suitable method to fabricate NV centers in diamond because low N and ^{13}C background concentrations are required to increase the decoherence times of the NV spin systems. On the other side, ion implantation in N-rich diamond samples already now allows for the creation of high density NV ensembles. Ensembles of emitters have great potential for quantum information processing (QIP), as the electromagnetic interaction strength is strongly enhanced[6], which increases the fidelity of state transfer and storage of quantum information[7]. The distributed storage of quantum information provides more temporal stability. Moreover, ensembles account for the modal structure of interacting light and allow for the storage of the temporal shape of qubit photons[8]. Therefore, in the current paper we present an extensive study on the effects of MeV He^+ ion implantation in type Ib diamond crystals and their suitability for ensemble QIP schemes.

Although it is clear from a theoretical point of view that NV ensembles in diamond are suitable for optical QIP, there are several optical and material-related key issues that are still debated and need to be fully understood if NV luminescence is to be consistently employed for quantum device architectures:

NV center density. A high conversion efficiency from nitrogen and vacancy defects to optically active NV centers is crucial to reach high NV densities, increasing the probability of an interaction. An active NV center can be created in a diamond crystal containing nitrogen and vacancy defects with thermal annealing at temperature ≥ 600°C. At such temperatures[9], the vacancies migrate to the nearest substitutional nitrogen atoms N_S, where their aggregation is energetically favorable[10]. The conversion efficiency is limited due to competitive processes such as the formation of other defects and vacancy-interstitial recombination. The present work determines an optimum implantation density for the creation of NV centers, while minimizing the effects of competitive processes.

Temporal stability of the NV center. The NV defect can exist in two charge-states (NV^- and NV^0) that have been correlated with λ=638 nm and λ=575 nm luminescence emissions, respectively[1]. Charge transfer[11–14] mechanisms lead to the conversion between NV^- and NV^0 centers (photo-ionization). This process appears experimentally as photobleaching of single emitters. The equilibrium between NV^- and NV^0 concentrations is determined by the presence of nitrogen donors in the lattice[15,16]. Owing to its Λ-shaped energy levels, the NV^- center is of primary interest for quantum computation, and a high NV^- / NV^0 ratio is desirable. In our analysis, we evaluate the dependence of this ratio both on implantation density and on optical excitation power to obtain the optimal parameters for a stable optical operation with NV^- centers. It is shown that the conversion to NV^0 can be completely suppressed even for medium-high implantation densities.

Inhomogeneous spectral broadening. The inhomogeneous broadening of the zero phonon line (ZPL) NV^- emission is usually reported as 750 GHz[1], which significantly exceeds the transform limit set by the inverse of the transition lifetime ($\sim$12 ns). Such large broadening is commonly attributed to variations in strain and electric fields within the diamond crystal, due both to impurities and structural defects[5]. Inhomogeneous broadening can lead to dephasing or undesired transitions in resonant QIP schemes, while off-resonant[8] or frequency-selective[17] schemes are less vulnerable to it.

The above mentioned issues are related with the fabrication of NV centers and it depends on the exact QIP scheme, which parameters are ideal for its implementation. In the present work, we relate our findings on NV center ensembles to a photonic quantum memory (Qmem) scheme that uses broadband pulses and an off-resonant transition[8]. This scheme utilizes a strong classical control pulse to absorb the qubit photon into a spin-wave excita-

tion in the material, which is a collective state of the ensemble. The read-out of the stored photon can be achieved using another strong classical control pulse. While the excited state inhomogeneous broadening of the ensemble is less important owing to the off-resonant nature of the transition, a very high density of absorbers is necessary to achieve a high quantum memory fidelity.

II. EXPERIMENTAL SETUP

A. Implantation and Annealing

The employed sample was an artificial diamond produced by Sumitomo. The crystals were cut and polished from large single crystals which were synthesized under ultra-high pressure and temperature (HPHT). All sides of the sample have 100 face orientation, and the crystal is classified as type Ib; the nitrogen concentration is $\sim 10-100$ ppm, as reported by the manufacturers.

The sample was implanted with 2 MeV He^+ ions on the MP2 microbeam line of the 5U NEC Pelletron accelerator at The University of Melbourne. Regions of 80×80 μm^2 were implanted in the central region of the sample at fluences ranging from 1×10^{13} ions cm^{-2} to $2{\times}10^{17}$ ions cm^{-2}, using a raster scanning ion beam which was focused to a micrometer-sized spot, providing optimal homogeneous ion fluence. The ion beam current ranged from $\sim$5 pA to $\sim$0.5 nA for different implantations, in order to maintain a reasonable implantation time ($\lesssim 10-30$ min). The ion fluence was measured by monitoring the Rutherford back-scattered ions, after having coated the sample with carbon in order to avoid charging; afterwards, the conductive coating was chemically etched. Figure 1a shows a transmission microscope image of the sample after ion implantation; the regions implanted at higher fluences are clearly visible because the high damage density makes the material opaque, while at fluences below $1{\times}10^{14}$ ions cm^{-2}, the implanted area are invisible to optical microscopy. Figure 1b shows the vacancy density profile of 2 MeV He^+ ions in diamond, calculated with "Transport of ions in matter" (TRIM) Monte Carlo simulation code[18]. The simulation takes into account both direct collisions and secondary recoil events, and the value of the atom displacement energy was set to 50 eV. Ion-induced damage causes a progressive amorphization of the crystalline structure with increasing ion fluences, which is localized mainly at the end of

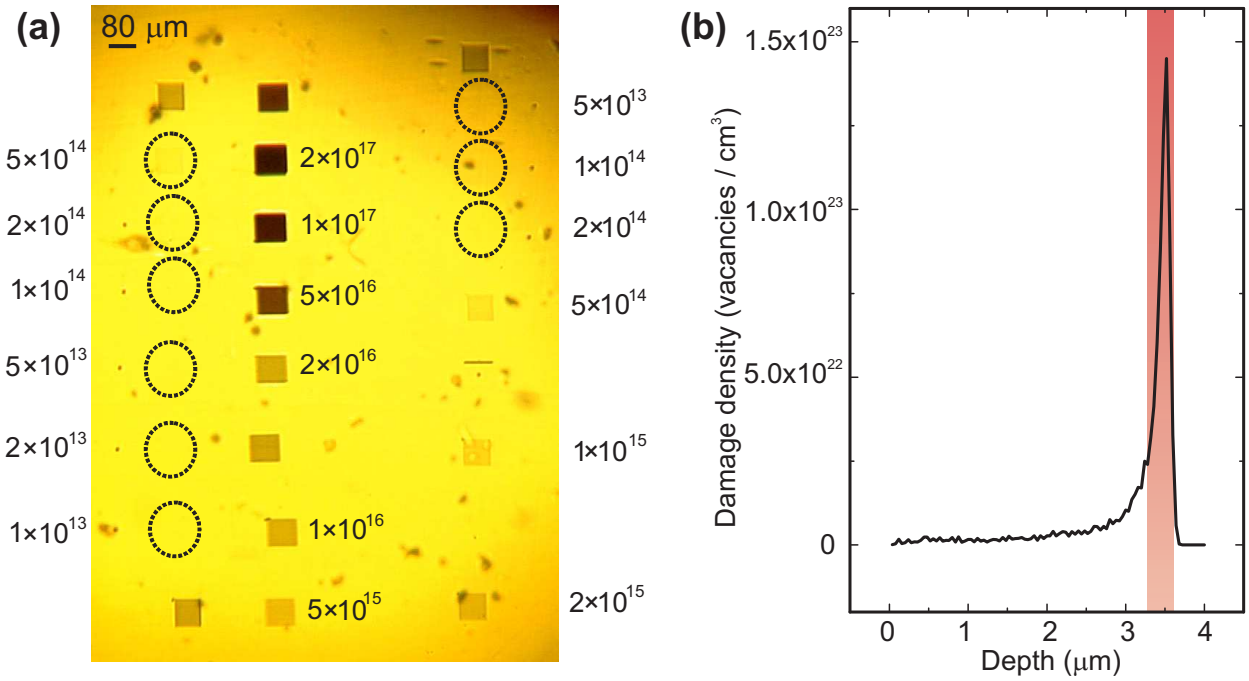

FIG. 1: **(a)** Transmission microscope image of the implanted sample; the 80×80 μm^2 implanted regions are labeled with the relevant ion fluences. Regions implanted at higher fluences are clearly visible because the damaged layer is opaque, while regions implanted at fluences below 10^{15} ions cm^{-2} are not visible. **(b)** TRIM Monte Carlo simulation of the damage density profile induced in diamond by 2 MeV He$^+$ ions, scaled for an implantation density of 1×10^{17} ions cm^{-2}; the damage density is concentrated at the end of the range, namely ~ 3.5 μm below the sample surface.

range of implanted ions (namely ~ 3.5 μm below the sample surface, as shown in Fig. 1b), where most of the nuclear collisions occur. The evolution of the amorphized structure upon thermal annealing depends critically on the damage density. In regions where the vacancy density is above a critical threshold, the diamond crystalline structure is permanently converted to a sp^2-bonded phase. When the damage density is below the critical threshold, thermal annealing has the effect of converting the amorphized structure back to the crystalline diamond phase, although residual point defects can form in the crystal. During the thermal annealing, vacancies (interstitials) become mobile in the crystal lattice at temperatures of ~ 600°C (< 100°C)[9]; in this process, they can either recombine with interstitial atoms, or form a vast range of luminescent centers, both isolated and paired with native impurities (N, B, Si, Ni, etc.)[1].

The sample was annealed for 1 hour at a temperature of 600°C in forming gas (4%

hydrogen in argon) atmosphere. The presence of hydrogen in the annealing atmosphere avoided high-temperature oxidation of the surface.

B. Optical Experiments

PL experiments were carried out using a Renishaw Raman apparatus with a Leica DMLM microscope. The sample was cooled to $T \sim 4$ K in an Oxford Instruments liquid helium flow cryostat, which could be positioned with micrometer precision. A reflecting microscope objective was employed for both excitation and signal collection, minimizing the effects of chromatic aberration. The lateral resolution of the system was ~ 2 μm and therefore much smaller than the size of the implanted regions. The photoluminescence was induced by $\lambda_{\rm exc} = 532$ nm light from a Suwtech single longitude mode laser.

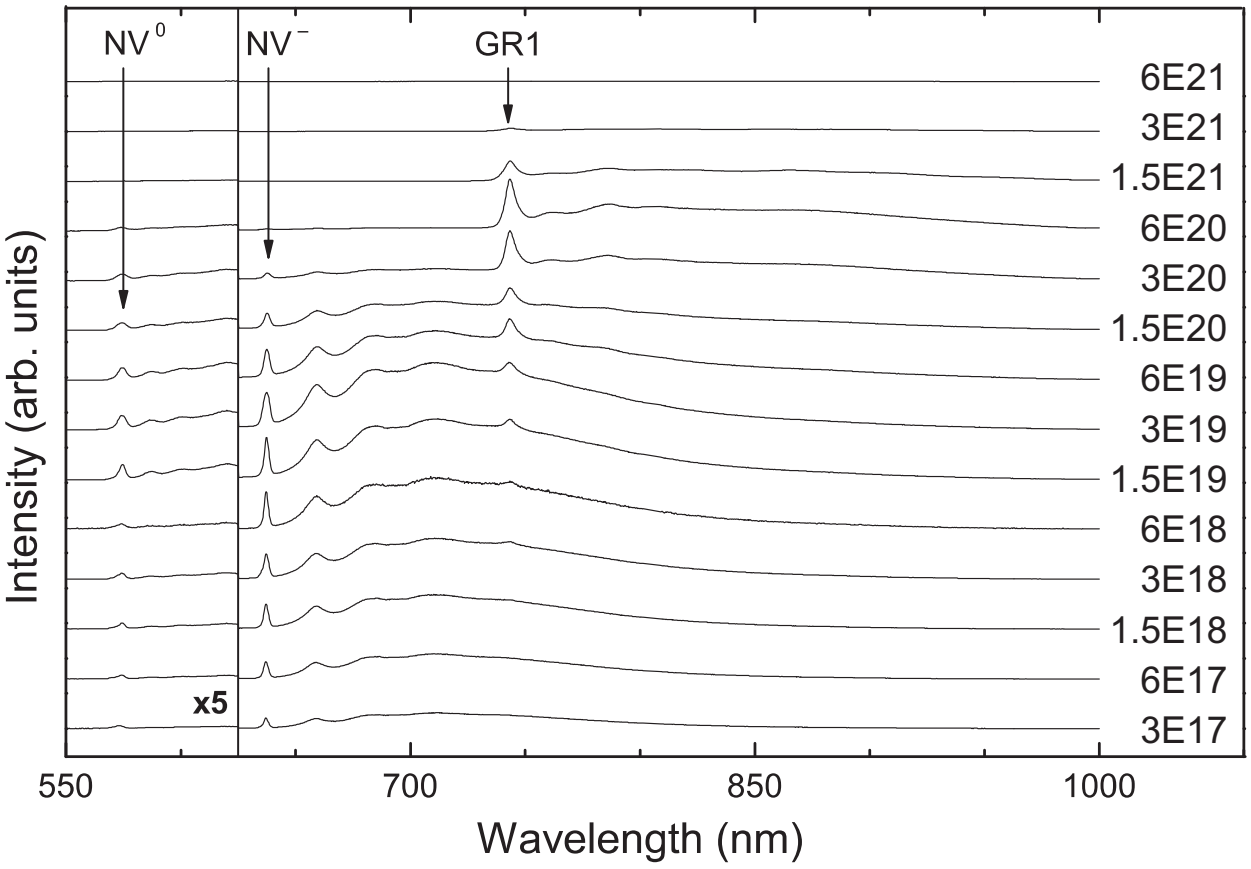

FIG. 2: PL spectra for various irradiation fluences. The left end of the spectra, containing the NV^0 peak, is magnified by a factor of 5. The vacancy density due to ion implantation in the cap layer (first 3 μm in figure 1b) is denoted on the right.

All spectra were acquired with the excitation and collection focus on the sample surface. Since the depth profile of the induced damage is non-uniform, slightly different focusing conditions might in principle affect the intensity of the PL signal; normalization to the intensity of the first order diamond Raman line is not possible since this is also significantly affected by ion-induced damage. Therefore, the reproducibility of the focusing conditions were tested by repeated measurements, from which variations of 2% were observed. Our spectra were recorded using the spectrometer with 300 and 1200 grooves/mm diffraction gratings. With $\lambda_{\rm exc} = 532$ nm laser excitation, the NV^0 PL emission and first order Raman line (Raman shift=1332 cm^{-1}, corresponding to $\lambda_{\rm Raman} = 572$ nm) partially overlap. The Raman emission has been subtracted from the NV^0 PL signal.

III. RESULTS

Figure 2 shows PL spectra from regions implanted at 14 different ion fluences, ranging from 2×10^{17} ions cm^{-2} to 1×10^{13} ions cm^{-2}. The NV^- and GR1 peaks (λ=637 nm and λ=742 nm, respectively) are clearly visible for most regions, although the GR1 doublet structure is not resolved due to an overlap of the two peaks attributed to inhomogeneous broadening. The NV^0 emission is at λ=575 nm and much weaker, but visible for some regions. The broad peaks on the red side of each ZPL peak arise from vibronic emission (phonon side bands).

A. PL Increase at low-medium implantation densities

Fig. 3 shows the intensities of the ZPL emissions from NV^-, NV^0 and GR1 centers as a function of the implanted ion fluence. In all cases, the PL intensities follow a non-monotonic trend. After a steady sub-linear increase, the NV^- and NV^0 emissions reach a maximum at fluence $F = 1 \times 10^{15}$ ions cm^{-2}, then steadily decrease until maximum fluence $F = 2 \times 10^{17}$ ions cm^{-2} is reached. In interpreting this trend, it is necessary to consider the number of vacancies created by implanted He^+ ions at various fluences, as compared with the native substitutional nitrogen concentration of $\sim 2 \times 10^{19}$ N_S cm^{-3}, corresponding to a 100 ppm concentration. By integration of the vacancy profile reported in Fig. 1b, one can estimate that each 2 MeV He^+ ion on average creates 38 vacancies in the diamond crystal.

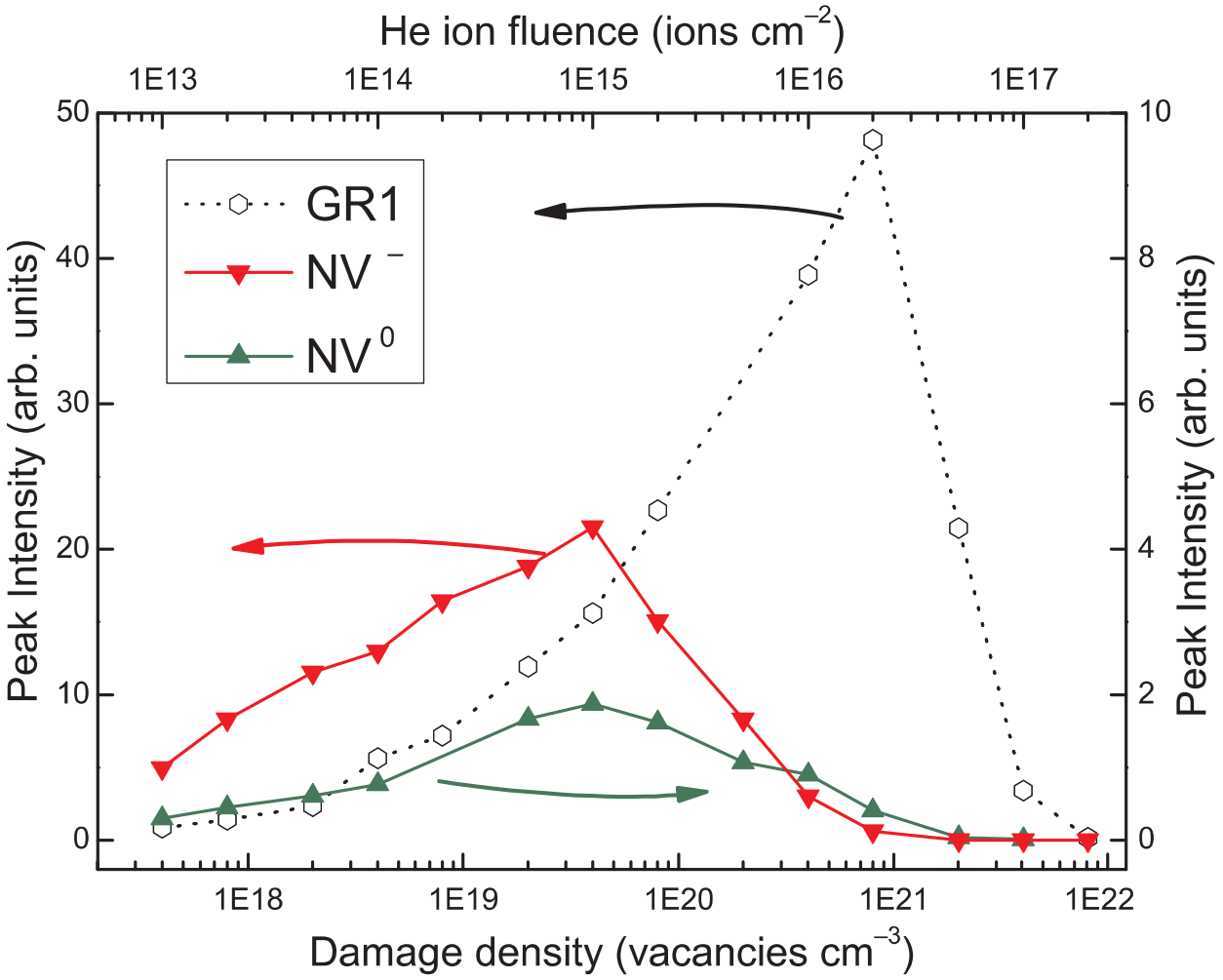

FIG. 3: (Color online.) Intensity of the NV^-, NV^0 and GR1 zero-phonon-line PL as a function of the implanted ion fluence (upper X scale) and correspondent vacancy density in the surface layer (lower X scale). The NV and GR1 emission intensities have a non-monotonic behavior, exhibiting maxima at 3×10^{19} vacancies cm^{-3} and 6×10^{20} vacancies cm^{-3} for NV and GR1, respectively.

The vacancy density profile is strongly non-uniform, with $\sim$ 80% of the vacancies being created in the last 0.5 μm of the total 3.5 μm ion damage range (highlighted in Fig. 1b). As visible in the transmission microscope image in Fig. 1a, regions implanted at fluences $F > 1 \times 10^{15}$ ions cm^{-2} turn opaque because of graphitization in the buried heavily-damaged layer 3.5 μm below the diamond surface. Therefore, at high ion fluences only the ~ 3 μm-thick surface layer is responsible for the enhanced PL signal, the end-of-range layer being optically opaque. At fluence $F = 1 \times 10^{15}$ ions cm^{-2}, about 3×10^{19} cm^{-3} vacancies are created in the surface layer with a relatively uniform depth distribution. Comparing this

density with the N_S density, one can conclude that, while at lower fluences the vacancies created by ion implantation can migrate to unpaired substitutional nitrogen during the thermal annealing, for $F \gtrsim 1 \times 10^{15}$ ions cm^{-2} the vacancy concentration exceeds the native N_S population and no further increase in PL signal can occur.

A confirmation for this interpretation can be found in the increase of the relative intensity of the GR1 emission with respect to the NV emission, as shown in Fig. 4. The GR1 emission is unambiguously attributed to isolated neutral vacancies in the diamond structure[1], and such a trend clearly indicates that isolated vacancies progressively exceed the NV centers population. It is worth remarking that the GR1 emission is measured at low (i.e. $< 1 \times 10^{15}$ cm^{-2}) ion fluences; this indicates that even where the native N_S concentration is higher than the vacancy concentration, not all the created vacancies get trapped at an N atom during thermal annealing. Therefore, we can qualitatively state that the N+V→NV conversion process has a limited efficiency, as previously reported[19].

B. PL decline at high implantation densities

As shown in Fig. 3, the NV^- and NV^0 intensities, after having reached a maximum, start decreasing at higher ion fluences. While at first a plateau behavior might be expected after the saturation of native N_S at $F = 1 \times 10^{15}$ ions cm^{-2}, it must be considered that the increasing damage density is detrimental to the NV emission, both in terms of the increasing optical absorption of the damaged crystal and of the competitive formation of other luminescent centers. Damage induced absorption is qualitatively visible in the microscope image (figure 1a) from regions implanted at fluences higher than $F = 1 \times 10^{15}$ ions cm^{-2}. From the data reported by Gippius *et al.*[20], it is possible to evaluate the absorption coefficient from ion damaged diamond: namely, a value of $\alpha \simeq 1.5 \times 10^4$ cm^{-1} is obtained for the highly-damaged buried layer of a crystal implanted with 350 keV deuterium at a fluence $F = 2 \times 10^{16}$ cm^{-2} and subsequently annealed. Under the assumption that the optical density scales linearly with the damage density, the TRIM Monte Carlo simulation of 2 MeV He induced damage for $F = 1 \times 10^{16}$ ions cm^{-2} can be used to roughly estimate a $\sim 35\%$ decrease of the PL signal due to optical absorption of both excitation laser light and induced luminescence in the 3μm thick surface layer. It is worth noticing that under the same assumptions, a $\sim 90\%$ decrease is estimated for the PL signal from the buried highly-damaged layer, thus justifying

our assumption that the measured PL signal is originated in the surface layer for high ion fluences. These simplistic estimations seem to be consistent with the measured 86% decrease of the signal at $F = 1 \times 10^{16}$ ions cm^{-2}, although they still underestimate the measured decrease of PL signal. Such a discrepancy could be attributed to the competitive formation of other PL centers. Since nitrogen is not mobile at T = 600°C, the natural candidates for such defects would be centers containing a single nitrogen atom bound either to multiple vacancies or interstitial C atoms. In both cases, an enhanced formation probability would be expected at higher implantation fluences. For higher ion fluences, the trend of the NV luminescence signal becomes more difficult to predict, as the increase of optical absorption and the formation of competitive centers have non-linear dependences with respect to the induced damage. The strong suppression of NV PL detected indicates that graphitization affects even shallow layers. Although it is likely that the NV density increases in the material, most of the NV centers are not optically accessible any more. Therefore, we can conclude that the optimum damage density for the formation of high-density NV ensembles in type Ib diamond is $\sim 3 \times 10^{19}$ vacancies cm^{-3}; such a density can be achieved with medium ion implantation fluences ($\sim 1 \times 10^{15}$ cm^{-2} for 2 MeV He$^+$ ions). If we assume a $\sim 3\%$ efficiency in the conversion from nitrogen / vacancy pairs to optically active NV centers upon thermal annealing[19], we can estimate a density of optically accessible active NV centers of $\sim 1 \times 10^{18}$ cm^{-3}.

In the context of the off-resonant Qmem scheme, a high ensemble density is necessary to reach a high fidelity. An ultrafast off-resonant transition[8] into a vibronic sideband of the electronic ground state of the NV$^-$ center could be used to implement a photonic quantum memory. For such ultra-high densities as in our sample, the transition could be realized for comparably low control-field laser powers (on the order of mW), despite the large detuning.

The GR1 emission also shows a non-monotonic trend, with a maximum at $F = 2 \times 10^{16}$ ions cm^{-2}. The abrupt decrease of the GR1 intensity at higher fluences can be explained with the damage-induced optical absorption: At $F = 5 \times 10^{16}$ ions cm^{-2} a $\sim 90\%$ decrease is expected from the surface layer, while the end-of-range layer is completely opaque. Renormalising the GR1 PL based on the absorption increase now delivers very strong luminescence. This is consistent with the fact that the creation of vacancies (which are responsible for the GR1 emission) keeps increasing at higher ion fluences, not being limited by the native N_S population, as the NV emission is.

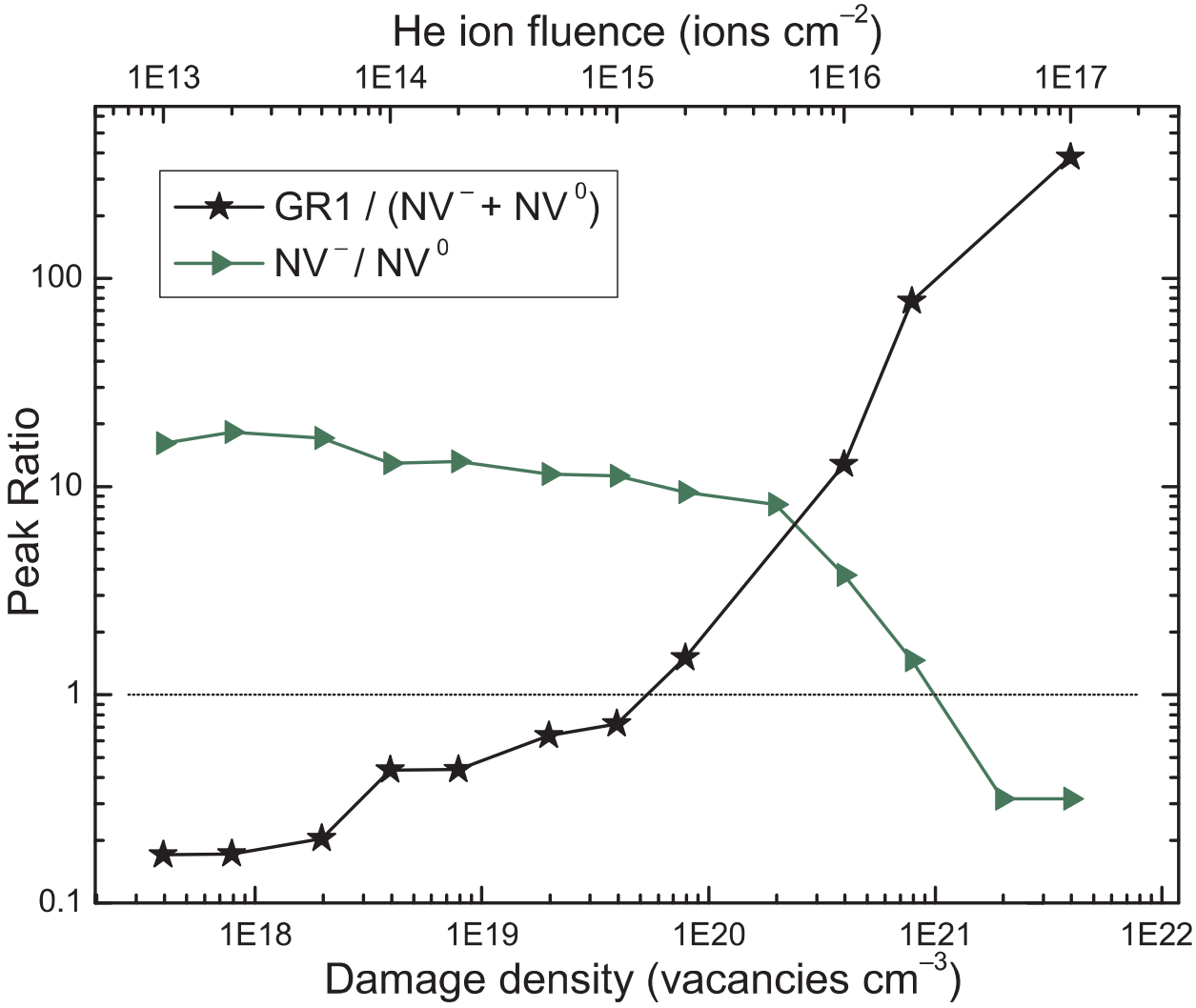

FIG. 4: (Color online.) Ratios of photoluminescence intensities. At about 3×10^{20} vacancies cm^{-3}, the fraction of NV^- decreases due to a lack of free negative charge in the material, provided by N_S (see text).

C. PL ratio of NV^- and NV^0

Few quantitative studies have been conducted on the relative NV^-/NV^0 intensity as a function of induced damage, using radiation sources (neutrons, electrons) that do not allow a straightforward estimation of the induced damage. In the context of QIP with NV^- centers, a very low ratio is desirable, as the occurrence of NV^0 disturbs optical transitions involving NV^- centers due to a spatial variation of the refractive index and temporal instability. This will be explained in more detail in the next section.

A common characteristic of the spectra reported here is the low intensity of the NV^0 emission with respect to the NV^- and GR1 emission. This is due to the fact that the type Ib diamond sample has a relatively high concentration of single substitutional nitrogen. Nitrogen acts as an electron donor in diamond with an ionization energy of 1.7 eV, while the ground state of of an NV^- center lies 2.58 eV below the conduction band[21]. The electrons provided by nitrogen donors are responsible for the conversion of nearby NV^0 centers to the charged NV^- state[15]; the process can be described by the reaction: $NV^0 + N_S \rightleftharpoons NV^- + N_S{}^+$. Studies carried out on samples with different concentrations of substitutional nitrogen proved that at low N_S concentration, the NV emission arises mainly from the neutral centers, while at high N_S, NV^- luminescence becomes largely predominant[16,22]. This is explained by statistical arguments with a variation of the Fermi level as a function of N doping concentration[12,13,23], or microscopically with the proximity of the NV defect to a nitrogen donor[11,15]. Our NV^-/NV^0 ratio of about 10 for low and medium implantation densities is consistent with previous reports[16], measuring an NV^-/NV^0 ratio of 3.3 for a CVD grown sample with a medium-high N_S density of 47 ppm.

Fig. 4 shows the evolution of the NV^-/NV^0 ratio with increasing implantation fluence. Although the NV^- and NV^0 emissions follow a similar non-monotonic trend with respect to the N_S saturation point at $F = 1 \times 10^{15}$ ions cm^{-2}, the NV^-/NV^0 ratio steadily decreases for increasing fluences, both in the low fluence and high fluence regimes. This behavior can be explained with the charge transfer process that determines the $NV^0 \leftrightarrow NV^-$ conversion. With increasing damage density, more nitrogen atoms pair with induced vacancies to form NV centers and fewer N_S donors are available to turn NV^0 centers into NV^- centers. This imposes a natural limit to the NV^- density achievable with high energy He ion implantation for a given sort of diamond. As the presence of NV^0 is unfavorable for QIP, the vacancy density created should not exceed the density of N_S of the sample.

D. Photo Chromism

Since the attribution of the 575 nm emission to the neutral state of the NV defect by Mita[23], conclusive work has demonstrated the photochromic behavior of the NV center[11,12,24]. NV^- centers can be discharged by high excitation powers (photoionization), leading to a significant increase of NV^0 centers present. Fig. 5 shows the normalized PL intensity of NV^0

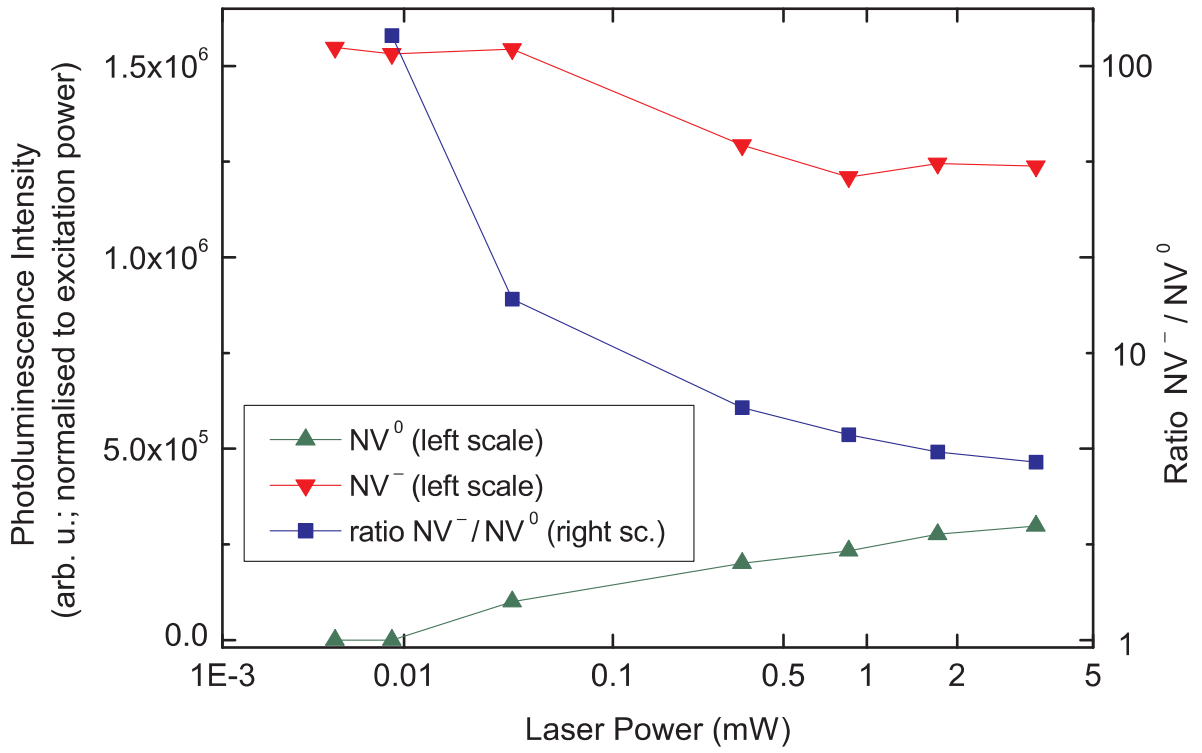

FIG. 5: (Color online.) Excitation power dependence of the NV PL (normalized to excitation power) and PL intensity ratio (vacancy density 1.5×10^{18} vacancies cm^{-3}). Photoionization leads to a strong increase in NV^0 signal for higher excitation powers. Ratio data points for which the NV^0 PL is not detectable have not been plotted.

and NV^- with respect to excitation power. For low power, the NV^0 emission vanishes, as all NV centers are negatively charged, whereas the fraction of neutral NV centers increases with increasing excitation power. A decrease of the signal strength of NV^- PL (normalized to laser power) occurs in the same way as NV^0 PL rises. At the powers used in our work (≤ 5 mW), PL saturation cannot be observed. With an excitation energy of 2.33 eV of our system, this ionization process can only occur via a resonant two-photon process by subsequent excitation and ionization of the NV^- center (ground state 2.58 eV below conduction band). The build-up time for the NV^0 PL signal has been reported as on the order of hundreds of μs[14]. At our peak excitation power, a conversion efficiency of up to 20 percent could be achieved, ranging similarly as reported by Manson *et al.*[14].

As the charge conversion process implies a change of resonance frequency and a loss of the electron to the conduction band with subsequent fast intraband decoherence, QIP schemes involving single NV^- emitters would most likely fail in the case of light induced

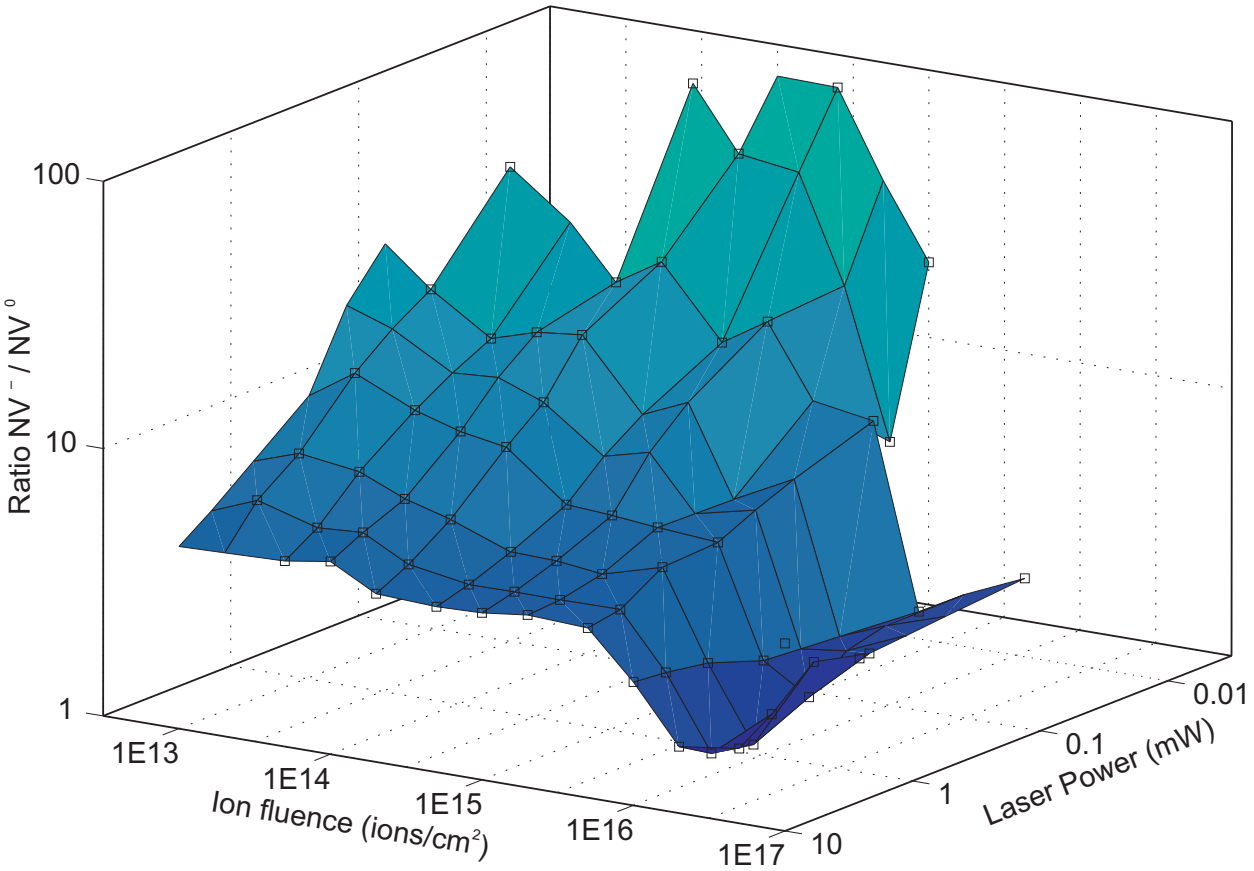

FIG. 6: (Color online.) PL ratio of NV^-/NV^0 with respect to implantation fluence and laser excitation power (logarithmic scales). The figure shows clearly that a high ratio can be reached even for medium-high implantation densities, indicating temporal stability of the NV^- centers in high-density ensembles. Data points for which the NV^0 PL is not detectable have not been plotted. In the figure, the surface has been obtained from the data points by spline interpolation. The black squares show the actual data points recorded. The PL linewidth (not plotted) remained constant at all laser powers within the accuracy of our detector (0.1 nm).

charged conversion. Schemes that involve ensembles of NV centers suffer a fidelity decline from a partial charge conversion of the contributing centers. It is therefore vital for QIP with NV^- ensembles to know the conditions for which the charge conversion of NV^- can be minimized. It is worth noting that the collective coupling strength of an ensemble for such high NV^- densities allows for control laser powers much lower than the laser powers used here for excitation. Moreover, the two-photon charge transfer process is likely to be strongly suppressed for off-resonant frequencies.

It is interesting to relate the photochromic behavior of the NV center to the ion implantation density. Fig. 6 shows a systematic analysis of the NV^-/NV^0 ratio as a function of implantation fluence and excitation power. As discussed above, at high implantation densities, the fraction of negatively charged NV centers decreases due to a lack of free electrons. Therefore, for very high implantation densities the NV^0 emission cannot be suppressed and the temporal stability of the NV^- center is not guaranteed. On the other hand, for lower implantation densities, the presence of NV^0 can be completely suppressed within the accuracy of our optical detection apparatus (at a signal to noise ratio for NV^- PL of over 100). Our systematic analysis (figure 6) shows that such a regime can even be reached for medium ion implantation fluences of up to 5×10^{14} ions cm^{-2}. Therefore, the technique of ion implantation of nitrogen rich HPHT diamond can be deployed to create high densities of NV^- centers without a detectable impact on their temporal stability.

E. Temperature Dependence

A temperature dependent study of the relative intensities of the different PL emissions was performed by collecting the photoluminescence signal from a region implanted at a fluence of 2×10^{14} ions cm^{-2} in the 8-280 K temperature range. As shown in Fig. 7, the PL spectra exhibit typical trends as a function of increasing temperature. The zero phonon lines become broader and less pronounced as a consequence of the relatively high electron-phonon coupling of the NV and GR1 centers with lattice vibrations at 65 and 36 meV, respectively[1].

The relative itensities of the NV^- and NV^0 zero phonon emissions do not exhibit strong temperature dependence, as previously noted by Manson *et al.*[14]. Remarkably, the relative intensity of the GR1 emission with respect to the (NV^- + NV^0) intensity follows a more pronounced trend, exhibiting a super-linear increase with increasing temperature (see Fig. 8a), while the relative NV^0 emission exhibit a marginal decrease (see Fig. 8b). Under the assumption that the electron-phonon coupling for NV and GR1 emissions have similar strengths, it is possible to interpret the measured trends as due to the redistribution of free electrons in the lattice between the defects as thermal energy is added to the system. Vacancies in diamond are an efficient trap for free electrons, therefore in type Ib crystals V^- is the favorable charge state[25,26]. While the position of the nitrogen donor level within the 5.47 eV energy gap is 1.7 eV below the conduction band (CB)[27], the ground states

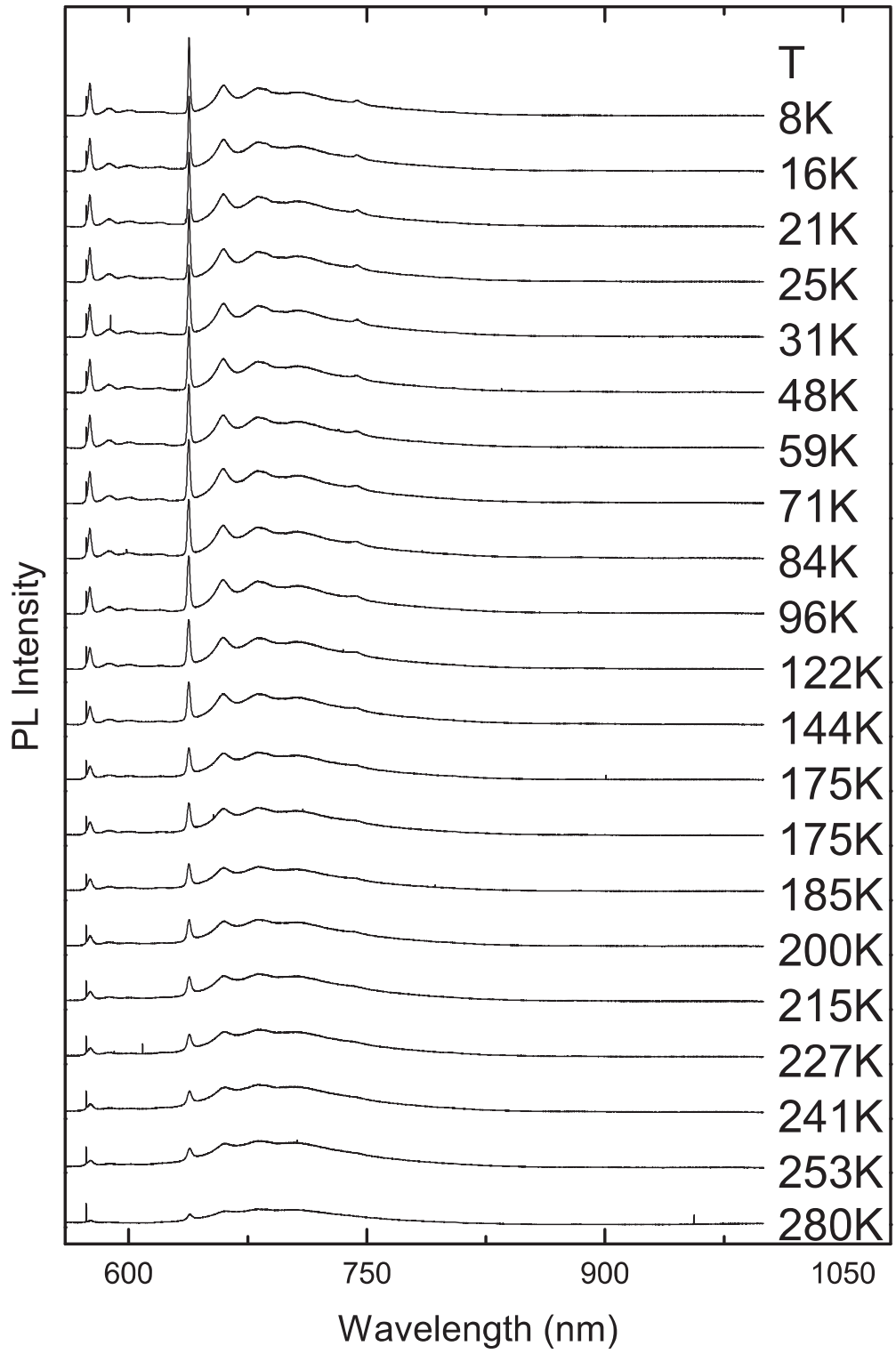

FIG. 7: Photoluminescence spectra collected from a region implanted at a fluence of 2×10^{14} ions cm^{-2} in the 8-280 K temperature range.

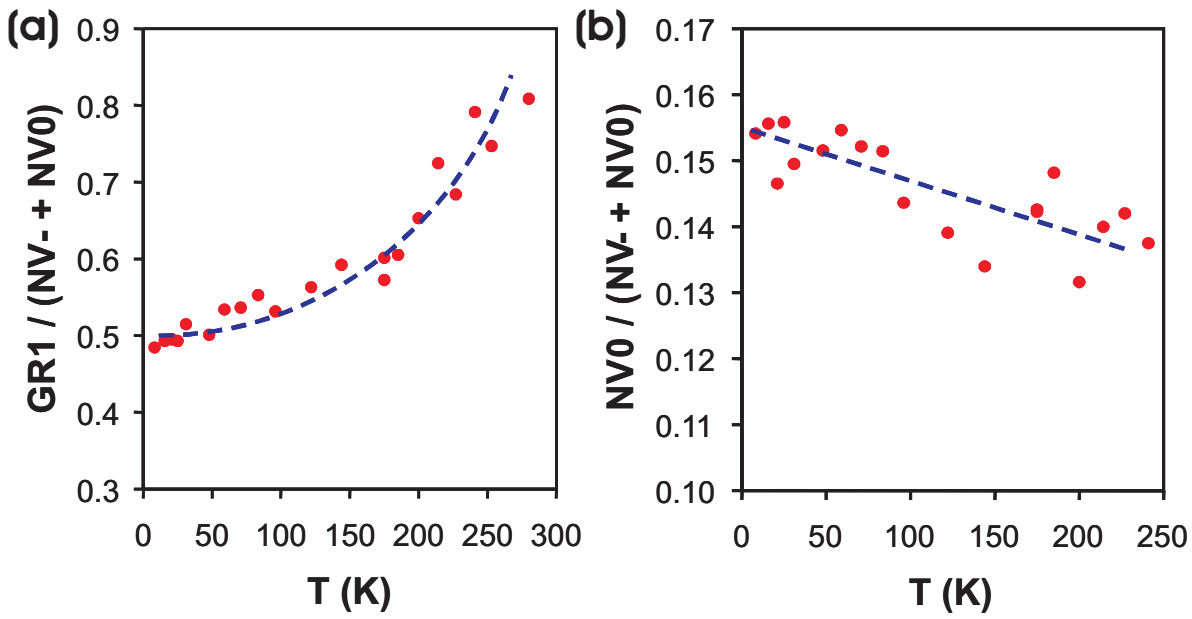

FIG. 8: (Color online.) **(a)** Ratio of the intensity of the GR1 ZPL emission and the total NV ZPL emission; a significant super-linear increase is observed as a function of temperature. **(b)** Ratio of the intensity of the NV^0 ZPL emission and the total NV ZPL emission; a marginal linear decrease is observed as a function of temperature. The dashed lines are not numerical fits, but guides for the eye.

of NV^-, NV^0 and charged vacancy centers lie respectively at $\sim E_{CB}-2.6$ eV[21], $\sim E_{CB}-2.8$ eV[24] and $\sim E_{CB}-3$ eV[28], as shown schematically in Fig.9. Therefore, we can qualitatively interpret the trends reported in Fig.8 with a thermally stimulated shift of the equilibrium of charge distribution between isolated vacancies and NV centers. In our interpretation, the relatively large nitrogen doping induces the negative charging of both NV centers and isolated vacancies, the trapping at the latter defects being energetically favored. As thermal energy is added to the system, the charge distribution shifts from the vacancy traps to higher energy levels, inducing the reactions: $(V^- \rightarrow V^0 + e^-)$ and $(NV^0 + e^- \rightarrow NV^-)$, hence the increase of neutral vacancy GR1 signal and the concomitant decrease of the NV^0 signal. The evidence that a marginal decrease of the NV^0 population corresponds to a significant increase of the V^0 population suggests that charges are re-distributed to other trapping centers which are not detected in our experiment: therefore we conclude that further investigation will be required to justify a detailed quantitative analysis.

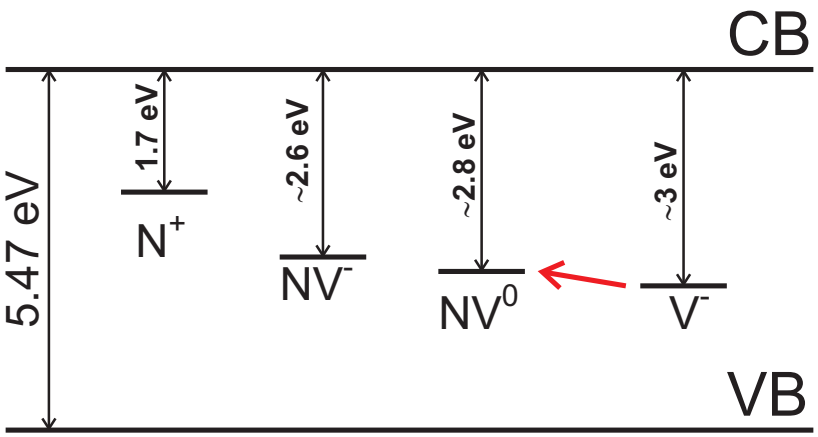

FIG. 9: (Color online.) Schematic diagram of the N^+, NV^-, NV^0 and V^- electronic levels within the diamond bandgap; the red arrow indicates the change transfer path used to explain the temperature dependence of the relative PL intensities.

This preliminary temperature-dependent investigation indicates that isolated vacancies limit the formation of active NV^- centers by trapping free carriers, and the electrons can be re-distributed within the optical centers as thermal energy is added to the system.

F. PL Peak Width

A large inhomogeneous broadening of the NV^- center ZPL has been reported for a great variety of samples. Recent research has shown a great interest in a reduction of this broadening, as a large inhomogeneous linewidth of an optical emitter limits its usability for reliable quantum information processing. For example, a quantum memory that stores a photon in an ensemble of strongly dispersed NV^- centers would dephase within picoseconds and controlled reversible inhomogeneous broadening[29] could not be realized in practice. On the other hand, inhomogeneous broadening causes less difficulties for off-resonant transitions, e.g. a Λ-transition as reported by Nunn *et al.*[8]. In this scheme, a large detuning also allows for the storage of ultrafast qubit photons. The stimulated transition would not be affected by the strong phonon sideband emission typical for the NV^- center.

The applicability of such techniques requires an exact understanding of the dynamics of the dephasing and decoherence mechanisms. Inhomogeneous broadening of NV^- PL emission has been attributed to local crystal field variations, the interaction with nearby

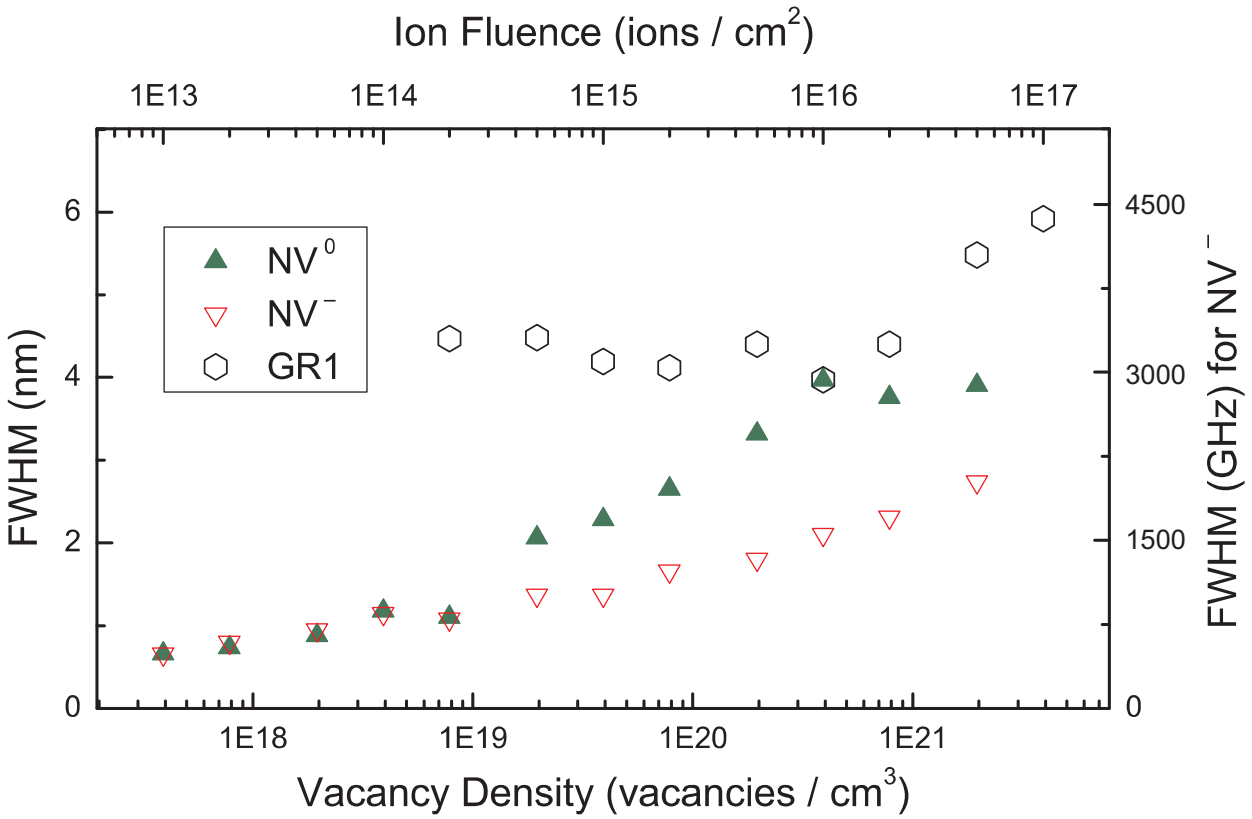

FIG. 10: (Color online.) PL peak widths of NV^0, NV^- and GR1 with respect to irradiation fluence (upper X axis) and relevant damage density in the surface layer (lower X axis). An increase of the damage of the center environment due to irradiation leads to a stronger broadening of the luminescence line.

nuclear spins (especially of the varying N and C isotopes), and charge fluctuations. Whereas the first two mechanisms are expected to be stable over timescales interesting for quantum information processing (at maximum, on the order of seconds), the charge carrier density fluctuates on much faster time scales. It is worth mentioning that this sort of inhomogeneous broadening thus has a temporal character, leading to a broad emission spectrum even of a single NV^- center. However, it has recently been shown[17] that a great reduction of the N_S density by a careful choice of the raw sample material and deliberate implantation of nitrogen molecules can lead to NV^- linewidths of about $\Delta\nu \sim 10$ GHz.

Despite the low temperatures, the linewidth of the NV^- peak in our sample is large. This is typical for NV centers created by ion implantation in impurity-rich HPHT diamond. The peak widths measured (full width at half maximum, FWHM) monotonically increase

from $\Delta\lambda = 0.66$ nm ($\Delta\nu \sim 480$ GHz) to $\Delta\lambda = 2.7$ nm ($\Delta\nu \sim 2$ THz) as a function of implantation fluence (see figure 10). We attribute this increase to the implantation induced damage to the crystal structure and an increase in stress. On the other hand, in the excitation power dependence measurements, we could not detect a change of the NV^- peak width for any implantation region. We therefore conclude that the increase of free charge carriers due to high laser illumination (1.6 kW cm^{-2}) has a small impact on the inhomogeneous linewidth compared to the broadening mechanisms prevalent in high nitrogen density diamond. QIP with such ZPL linewidths is possible for off-resonant transitions, whereas the above mentioned method of nitrogen implantation in pure diamond seems favorable for resonant QIP schemes. Although smaller densities are sufficient for a high fidelity of resonant transitions, research has yet to show whether nitrogen implantation will be capable of creating sufficiently high density ensembles of NV^- centers.

IV. CONCLUSION

We have analyzed a variety of optical properties of a type-Ib diamond sample, which has been systematically He implanted over a wide range of fluences. At low and medium fluences, the PL signal from NV centers increases with the fluence, whereas at high fluences absorption and competing processes lead to a decline of the NV luminescence. The ratio of NV^-/NV^0 fluorescence decreases for high implantation densities, as the density of residual nitrogen atoms which act as electron donors decreases. We have analyzed this ratio with respect to irradiation density and crystal damage, temperature, and excitation power. The concurrent examination by ion implantation fluence and excitation power reveals suitable conditions for which the NV^- center is a temporally stable absorber in the solid state, as the charge-conversion due to photoionization can be strongly suppressed. The results have been reviewed in the context of QIP. Due to the ultra-high densities of the NV center ensembles created, the coupling strength suffices for off-resonant Λ-transitions which could be used for a photon memory.

V. ACKNOWLEDGMENTS

The authors gratefully acknowledge support by the QIPIRC and EPSRC (grant number GR/S82176/01). FW thanks Toshiba Research Europe for their support. This work was supported by the Australian Research Council, the Australian government and by the US National Security Agency (NSA), Advanced Research and Development Activity (ARDA), and the Army Research Office (ARO) under contract number W911NF-05-1-0284 and DARPA QUIST. We thank Martin Castell, Andrew Briggs and Chris Salter supporting us in the analysis of the sample.

---

* Electronic address: felix.waldermann@physics.ox.ac.uk

[1] A. M. Zaitsev, *Optical Properties of Diamond* (Springer-Verlag Berlin Heildelberg, 2001).

[2] A. Gruber, A. Drabenstedt, C. Tietz, L. Fleury, J. Wrachtrup, and C. von Borczyskowski, Science **276**, 2012 (1997).

[3] A. Beveratos, R. Brouri, T. Gacoin, A. Villing, J.-P. Poizat, and P. Grangier, Phys. Rev. Lett. **89**, 187901 (2002).

[4] F. Jelezko, T. Gaebel, I. Popa, M. Domhan, A. Gruber, and J. Wrachtrup, Phys. Rev. Lett. **93**, 130501 (2004).

[5] A. D. Greentree, P. Olivero, M. Draganski, J. R. R. E. Trajkov, P. Reichart, B. C. Gibson, S. Rubanov, S. T. Huntington, D. N. Jamieson, and S. Prawer, J. Phys. C **18**, S825 (2006).

[6] M. D. Lukin, M. Fleischhauer, R. Cote, L. M. Duan, D. Jaksch, J. I. Cirac, and P. Zoller, Phys. Rev. Lett. **87**, 037901 (2001).

[7] K. Surmacz, J. Nunn, F. C. Waldermann, Z. Wang, I. Walmsley, and D. Jaksch (2006), to appear in Phys. Rev. A.

[8] J. Nunn, I. A. Walmsley, M. G. Raymer, K. Surmacz, F. C. Waldermann, Z. Wang, and D. Jaksch (2006), preprint arxiv/quant-ph/0603268.

[9] L. Allers, A. T. Collins, and J. Hiscock, Diamond and Related Materials **7**, 228 (1998).

[10] K. Iakoubovskii and G. J. Adrianenssens, J. Phys. C **13**, 6015 (2001).

[11] T. Gaebel, M. Domhan, C. Wittmann, I. Popa, F. Jelezko, J. Rabeau, A. Greentree, S. Prawer, E. Trajkov, P. Hemmer, et al., Applied Physics B: Lasers and Optics **82**, 243 (2006).

[12] K. Iakoubovskii, G. J. Adrianssens, and M. Nesladek, J. Phys. C **12**, 189 (2000).

[13] I. N. Kupriyanov, V. A. Gusev, Y. N. Pal'yanov, and Y. M. Borzodov, J. Phys. C **12**, 7843 (2000).

[14] N. B. Manson and J. P. Harrison, Diamond and Related Materials **14**, 1705 (2005).

[15] A. T. Collins, J. Phys. C **14**, 3743 (2002).

[16] A. Wotherspoon, J. Steeds, B. Catmull, and J. Butler, Diamond and Related Materials **12**, 652 (2003).

[17] C. Santori, D. Fattal, S. M. Spillane, M. Fiorentino, R. G. Beausoleil, A. D. Greentree, P. Olivero, M. Draganski, J. R. Rabeau, P. Reichart, et al. (2006), preprint arxiv/condmat/0602573.

[18] J. F. Ziegler, J. P. Biersack, and U. Littmark, *The Stopping and Range of Ions in Solids* (Pergamon, New York, 1985).

[19] J. R. Rabeau, P. Reichart, G. Tamanyan, D. N. Jamieson, S. Prawer, F. Jelezko, T. Gaebel, I. Popa, M. Domhan, and J. Wrachtrup, Appl Phys Lett **88**, 023113 (2006).

[20] A. A. Gippius, R. A. Khmelnitsky, V. A. Dravin, and A. V. Khomich, Physica B **308-310**, 573 (2001).

[21] J. Steeds, S. Charles, J. Davies, and I. Griffin, Diamond and Related Materials **9**, 397 (2000).

[22] T. A. Kennedy, J. S. Colton, J. E. Butler, R. C. Linares, and P. J. Doering, Appl Phys Lett **83**, 4190 (2003).

[23] Y. Mita, Phys. Rev. B **53**, 11360 (1996).

[24] K. Iakoubovskii, G. J. Adriansseens, M. Nesládek, and L. M. Stals, Diamond and Related Materials **8**, 717 (1999).

[25] G. Davies, Nature **269**, 498 (1977).

[26] G. Davies, S. C. Lawson, A. T. Collins, A. Mainwood, and S. J. Sharp, Phys. Rev. B **46**, 13157 (1992).

[27] L. A. Vermeulen and G. G. Farrer, *Diamond Research* (Industrial Diamond Information Bureau, London, 1975).

[28] S. C. Lawson, D. Fischer, D. C. Hunt, and M. E. Newton, J. Phys. C **10**, 6171 (1998).

[29] M. Nilsson and S. Kroll, Opt. Commun. **247**, 393 (2005).